Environmental Pollution 231 (2017) 1–12

Contents lists available at ScienceDirect

Environmental Pollution

journal homepage: www.elsevier.com/locate/envpol

Relationship between reactive oxygen species and water-soluble organic compounds: Time-resolved benzene carboxylic acids measurement in the coastal area during the KORUS-AQ campaign☆

Min-Suk Bae [a, b], James J. Schauer [b], Taehyoung Lee [c], Ju-Hee Jeong [d], Yoo-Keun Kim [d], Chul-Un Ro [e], Sang-Keun Song [f], Zang-Ho Shon [g, *]

[a] Department of Environmental Engineering, Mokpo National University, Muan 58554, Republic of Korea
[b] Department of Civil & Environmental Engineering, University of Wisconsin-Madison, Madison 53705, USA
[c] Department of Environmental Science, Hankuk University of Foreign Studies, Gyeonggi 17035, Republic of Korea
[d] Department of Atmospheric Sciences, Pusan National University, Busan 46241, Republic of Korea
[e] Department of Chemistry, Inha University, Incheon 22212, Republic of Korea
[f] Department of Earth and Marine Sciences, Jeju National University, Jeju 63243, Republic of Korea
[g] Department of Environmental Engineering, Dong-Eui University, 47340, Republic of Korea

ARTICLE INFO

Article history:
Received 20 April 2017
Received in revised form
20 July 2017
Accepted 29 July 2017

Keywords:
ROS
Benzene carboxylic acid
WSOC
OC

ABSTRACT

This study investigated the relationship between water-soluble organic compounds of ambient particulate matter (PM) and cellular redox activity collected from May 28 to June 20 of 2016 at the west coastal site in the Republic of Korea during the KORea-US Air Quality (KORUS-AQ) campaign. Automatic four-hour integrated samples operated at a flow rate of 92 L per minute for the analysis of organic carbon (OC), water-soluble organic carbon (WSOC), elemental carbon (EC), water-soluble ions (WSIs), and benzene carboxylic acids (BCAs) were collected on a 47 mm quartz fiber filter. The influence of atmospheric transport processes was assessed by the Weather Research and Forecasting (WRF) model. OC, EC, WSOC, and BCA were determined by SUNET carbon analyzer, total organic carbon (TOC) analyzer, and liquid chromatography-mass spectrometry mass spectrometry (LC-MSMS), respectively. Twenty-four-hour integrated samples were collected for reactive oxygen species (ROS) analysis using a fluorogenic cell-based method to investigate the main chemical classes of toxicity. The results illustrate that WSOC and specific water-soluble species are associated with the oxidative potential of particulate matter. Pairwise correlation scatterplots between the daily-averaged WSOC and ROS (r^2 of 0.81), and 135-BCA and ROS (r^2 of 0.84), indicate that secondary organic aerosol production was highly associated with ROS activity. In addition, X-ray spectral analysis, secondary electron images (SEIs) of $PM_{2.5}$ particles, and dried deposits of particles collected during high ROS concentration events clearly indicate that water-soluble organic aerosols are major contributors to $PM_{2.5}$ mass. This study provides insight into the components of particulate matter that are drivers of the oxidative potential of atmospheric particulate matter and potential tracers for this activity.

1. Introduction

A number of studies of organic aerosols have been carried out to understand the organic aerosol characteristics in particulate matter (PM) and associated sources over various regions (Agudelo-Castañeda et al., 2017; Belis et al., 2011; Hasheminassab et al., 2013; Pant et al., 2014). It has been found that secondary OC (SOC) generally contributes more than half of the measured OC, based on ratios of organic carbon to elemental carbon (OC/EC), and water-soluble organic carbon (WSOC) to OC (WSOC/OC) (Bae et al., 2006; Pathak et al., 2011). Quantifying the contribution of SOC to OC is of importance to identify the PM originations. Previous works have presented that SOC consists of aged compounds (i.e., aldehyde, carboxylic acid, amine, etc.), which have high solubility (Saxena and Hildemann, 1996; Sullivan et al., 2004). Accordingly,

☆ This paper has been recommended for acceptance by Maria Cristina Fossi.
* Corresponding author.
E-mail address: zangho@deu.ac.kr (Z.-H. Shon).

http://dx.doi.org/10.1016/j.envpol.2017.07.100
0269-7491/

measurements of the WSOC have been utilized to contribute SOC to OC from biomass burning aerosols (Stone et al., 2009; Sullivan et al., 2004). In particular, the ratio of WSOC to OC presented a strong positive correlation with the acid concentrations in the Northeast Asia regions (Pathak et al., 2011). Such a high WSOC fraction in OC can be postulated to be linked to the conversion of OC to WSOC, which is due to heterogeneous acid catalyzed chemistry.

Dicarboxylic acids and saccharidic compounds (e.g., levoglucosan) are two major classes in WSOC over the northwestern Pacific region (Simoneit et al., 2004). Dicarboxylic acids and related polar compounds are also important components in WSOC due to the hygroscopic property (Jung et al., 2011). Dicarboxylic acids are mainly produced by photochemical processes of the precursor species emitted from biomass burning and vehicular exhaust, while saccharidic compounds originate from biomass burning and plant material (Bae et al., 2012; Jordan et al., 2006; Kawamura et al., 1996). A recent study showed that biomass burning accounted for 16% and 23% of WSOC in summer and winter, respectively (Yan et al., 2015). The other study presented that the daily concentration of biomass burning to WSOC was as little as 20% of WSOC (Snyder et al., 2009). In addition, benzoic acid (BA), a secondary product due to photochemical reaction of aromatic hydrocarbons, has been shown to exist in PM (Ho et al., 2011). Originations of BA are mainly from a variety of anthropogenic emissions, such as automobiles and burning fuel oil (Rogge et al., 1997). The decomposition and/or photodegradation products of alkyl-substituted benzenes from petroleum hydrocarbons caused significant levels of benzene carboxylic acids (BCAs). Naphthalene and methylnaphthalenes are the precursors of phthalic acid derived from the photooxidation of aromatic organic compounds (Kautzman et al., 2010; Kawamura and Kaplan, 1987; Kleindienst et al., 2012). Time-resolved organic acid concentrations in PM are very of importance in understanding their photochemical (e.g., aging) and atmospheric transport processes (Bae et al., 2014). Therefore, their characterizations on the molecular level can further strengthen our understanding of organic aerosols in highly polluted conditions, such as Asian outflows.

Many epidemiological studies have illustrated that the extent of PM exposure causes strong relationships with public health (e.g., neurodegenerative, respiratory, and cardiovascular diseases) (Campbell et al., 2005; Morgan et al., 2011). Reactive oxygen species (ROS) on the basis of the cell redox status is widely used methodology to understand PM toxicity (Xia et al., 2004; Verma et al., 2012). WSOC greatly depends on the natural and anthropogenic originations in variety of atmospheric conditions. Therefore, to develop a toxicity-related understanding of the originations of WSOC is indispensable due to its negative effects on human health in SOC. Several epidemiological studies have reported toxicity associations of both soluble and insoluble species (Wang et al., 2013). The correlations between cellular reactive oxygen/nitrogen species production and organic species (e.g., WSOC) in summer highlight the importance of understanding the contributions of organic aerosols, especially the contribution of photochemically driven summertime SOA to PM-induced health effects (Tuet et al., 2016). Hamad et al. (2015) presented that a moderate correlation between ROS and WSOC, which is related to biomass burning. However, the toxicity of time-resolved WSOC at a molecular level is rarely studied. This information is important because it allows useful information to be gained on the health associated sources of Asian aerosols.

The aim of this study is to investigate the relationship between water-soluble organic compounds and cellular redox activity in $PM_{2.5}$ samples collected from May 28 to June 20 of 2016 at a west coastal site in the Republic of Korea. Four-hour integrated samples automatically collected for the measurements of OC and EC, WSOC, water-soluble ions (WSIs), and benzene carboxylic acids (BCAs) were analyzed by SUNET carbon analyzer, total organic carbon (TOC) analyzer, ion chromatography (IC), and liquid chromatography-mass spectrometry mass spectrometry (LC-MSMS), respectively. The Weather Research and Forecasting (WRF) model and back trajectory analysis determined the influences of atmospheric transport processes. The macrophage ROS assay using a fluorogenic cell-based method from rat alveolar macrophages were analyzed. Correlation between ROS and PM chemical components was investigated to identify the main classes of $PM_{2.5}$ toxicity.

2. Experimental methods

2.1. Time-resolved $PM_{2.5}$ sequence sampling

Time-resolved $PM_{2.5}$ sampling was carried out over Anmyeon Island in South Korea from May 28 to June 20 in 2014. The Anmyeon site (36° 32′ N; 126° 19′ E, 46 m above sea level (ASL)), which receives both marine and continental air masses by local circulation and regional and long-range transport processes depending on the prevailing meteorological conditions (Jeon et al., 2015), has been operated as a clean background site and a Global Atmosphere Watch supersite (Supplemental Fig. S1). Four-hour integrated automatic sequence samples for OC, EC, WSOC, WSIs, and BCAs analysis were collected on a 47 mm quartz fiber filter (Pallflex, 2500QATUP, Pall Corp., USA) downstream of $PM_{2.5}$ cyclones (URG-2000-30ENB, URG Corp., USA) that operated at a flow rate of 92 L per minute (lpm) using a custom-made $PM_{2.5}$ sequential sampler (APM Inc., Korea) (Supplemental Fig. S1). The flow rate through the medium volume (vol.) samplers were controlled using a mass flow controller (MFC) (precision of 92 ± 1 lpm) equipped with timers to start and stop automatic sample collection for every four hours during sampling periods. In addition, the 24-h low vol. sampler was operated for the ROS and trace element analyses. The results using the 24-h low vol. sampler have been compared with four-hour time-resolved concentrations. Samples using the 24-h low vol. sampler were collected downstream of a $PM_{2.5}$ impactor (BMI Inc., USA) that operated at a flow rate of 16.7 lpm using critical orifices, which were checked using a dry gas calibrator (Defender 510, Mesa Labs, Inc., USA). The 24-h integrated sampler was equipped with two sample trains. One train consisted of a single 47 mm Teflon filter (PTFE, R2PJ047, Pall Corp., USA) for ROS and trace elements. The other train consisted of a replaceable parallel charcoal-impregnated organics denuder (Sunset Laboratory Inc., USA), followed by a 47 mm quartz fiber filter. OC, EC, WSOC, and BCAs were analyzed from 24-h samples collected on a quartz filter.

2.2. Reactive oxygen species (ROS)

The fluorogenic cell-based macrophage ROS activity was determined from the Teflon filter (Landreman et al., 2008). Briefly, rat alveolar macrophages (NR8383, American Type Culture Collection) were utilized to investigate the production of ROS using 2,7-dichlorodihydrofluorescein diacetate as the fluorescent probe. After converting to a highly fluorescent compound of dichlorofluorescein, the fluorescence intensity (i.e., 504 nm excitation and 529 nm emission) was used. The detailed methodology in this study were explained in supplemental information.

2.3. $PM_{2.5}$ chemical analysis

The carbonaceous analyses were performed using standardized thermal optical transmittance (TOT) OC and EC analyzer (Sunset Laboratory Inc., USA) (Bae et al., 2004a, 2004b). Briefly, the filter

was heated based on the National Institute for Occupational Safety and Health (NIOSH) protocol. The loaded filter was heated to 840 °C under pure helium gas to release the organic compounds and pyrolysis products from PM on the filter. The desorbed carbon fragments converted to CH_4 from oxidized CO_2 were measured by a flame ionization detector (FID). An internal standard (i.e., CH_4) and external standard (i.e., sucrose) were injected for quantification. The strength of laser transmittance can determine the split between OC and EC. The average recovery was 1.00 ± 0.02. Field blank test without collecting aerosols was performed from each four-hour and 24-h integrated samplers to determine the noise and contamination. Duplication analysis for PM samples was performed at every fifth sample. To determine the WSOC and WSIs, the remaining areas of samples after OC and EC analyses were extracted. The filter extraction process involved placing the filter in previously baked pyrex glass vials with 20 mL of milli-Q water each and then placing the vials in an ultrasonic bath at 20 °C controlled by a low-temperature circulator (EYELA, Tokyo Rikakikai Co., Japan) for 120 min. All the water extracts were filtered by a 0.45 μm membrane filter (hydrophilic PTFE 0.45 μm pore size, Advantec, Japan) and then analyzed for sodium (Na^+), ammonium (NH_4^+), potassium (K^+), calcium (Ca^{2+}), magnesium (Mg^{2+}), chloride (Cl^-), nitrate (NO_3^-), and sulfate (SO_4^{2-}) using ion chromatography (Metrohm 883, Switzerland). Metrohm Metrosep A Supp-5 with eluent of 3.2 mM Na_2CO_3 and 1.0 mM $NaHCO_3$, and Metrohm Metrosep C4-250 columns with 1.7 mM HNO_3 and 0.7 mM dipicolinic acid, were used for the analysis of anion and cation compounds, respectively. The injection volume was 250 μl. The method detection limit (MDL) was determined as 3.14 (i.e., pi) times the standard deviation of the lowest detected standard concentrations. The determined MDL for Na^+, NH_4^+, K^+, Ca^{2+}, Mg^{2+}, Cl^-, NO_3^-, and SO_4^{2-} was 2, <1.0, 3, 10, 11, 3, <1.0, and <1.0 ppb, respectively. Sample precision was less than 3.0% for all ionic compounds. The remaining portions of water extracts were analyzed by TOC analyzer (Sievers 900, GE, USA) for WSOC. The TOC analyzer measures WSOC by subtracting inorganic carbon into CO_2 without ultraviolet light (UV) from all organic carbon into CO_2 with ammonium persulfate and UV. The conductivity through a semipermeable membrane was measured. However, the inorganic carbon concentrations cause higher analytical uncertainties. So, an inorganic carbon remover (ICR) was installed to reduce the interference of inorganic carbon to determine WSOC concentrations. The external sucrose standard was analyzed for quantification. The average recovery was 1.00 ± 0.03. Five trace elements (i.e., Al, Si, Fe, Cu, and Mn) were determined (i.e., average of three times analysis) using a portion of Teflon filter by an energy-dispersive X-ray fluorescence (EDXRF) (S2 PUMA, Bruker, Germany) analyzer. Briefly, an X-ray tube producing up to 50 W power and 50 kV excitation voltage with silicon drift detector (SDD) was utilized for excellent energy resolution. The National Institute of Standards and Technology (NIST) Standard Reference Materials 2783 (SRM2783) were analyzed for element quantifications.

2.4. Sensitive analysis of underivatized benzene carboxylic acids (BCAs)

Time-resolved analysis of underivatized BCAs is challenging, due to the difficulty in detecting these small amounts of polar analytes. The rest of the extracts after analysis of the WSOC and WSIs were analyzed for underivatized BCAs using LC-MSMS. After an internal standard injection of phthalic acid (D4), the extracts were completely dried by a freeze dryer (il-Shin BioBase, South Korea). The milli-Q water of 1.0 ml was spiked into the dried sample tube for the final extract volume. Hydrophilic interaction LC used an Eclipse XDB-C18 4.6 mm ID x 150 mm (5 μm) column as stationary phase with 10 mM ammonium acetate and acetonitrile in milli-Q water. It was combined with MSMS in multiple reaction monitoring (MRM) mode for the separation and detection of five underivatized BCAs (i.e., phthalic acid (12BCA), terephtalic acid (14BCA), trimellitic acid (124BCA), trimesic acid (135BCA), and pyromellitic acid (1245BCA)). The values of product ions from precursor ions were 165.1, 164.8, 165.2, 209.1, and 165.0 m/z for 12BCA, 14BCA, 124BCA, 135BCA, and 1245BCA, respectively. Regression coefficients of determination for seven point calibrations from 0.998 to 0.999. Absolute MDLs were in the range of 1.72–4.61 pg/m^3. Supplemental Tables S1 and S2 show the best analytical conditions in LC-MSMS and the final mass fragment transitions of quantification purpose (i.e., fragmentor voltage, collision energy, quantifier, and qualifier ions).

2.5. Scanning electron microscopy/energy-dispersive X-ray spectrometry (SEM/EDX) analysis

For SEM/EDX analysis of $PM_{2.5}$ particles, PM samples were collected on Al foils using a three-stage cascade Dekati impactor (Dekati Ltd., Finland). Using scanning electron microscopy (JSM-6390, JEOL) equipped with an Oxford Link SATW ultrathin window energy-dispersive X-ray (EDX) detector, the $PM_{2.5}$ samples were analyzed (Geng et al., 2009, 2014; Ro et al., 2003; Ro et al., 2004). The detailed SEM/EDX procedures in this study were presented in supplemental information.

2.6. Meteorological model

The Weather Research and Forecasting (WRF) model (Version 3.4) was used for the meteorological analysis. The WRF includes fully compressible nonhydrostatic equations with a hydrostatic option. The mother domain (D01) (e.i., 42 sigma vertical levels, 61 × 47 grid cells, and a horizontal resolution of 81 km) and the finer domains (D02 and D03), which are including horizontal resolutions of 27 km and 9 km covering 30.18–43.98 °N/115.99–133.85 °E and 32.81–38.86 °N/123.42–130.12 °E, respectively, were investigated. The WRF physical options were the WRF double-moment 6-class (WDM6) microphysics scheme, RRTMG longwave and shortwave scheme, revised MM5 surface layer scheme, Noah land surface model, Yonsei University planetary boundary layer scheme, and Kain-Fritsch cumulus parameterization (for the mother domain). The initial/lateral boundary conditions were generated by interpolating the National Center for Environmental Prediction (NCEP) final analysis (FNL) fields and the sea surface temperature (SST) data. The objective analysis technique (OBSGRID) was used to improve the first-guess gridded analysis using surface (ds461.0) and upper-level (ds351.0) observations. To analyze the wind fields for all event periods, the WRF simulations were conducted for 23 days from 00 UTC on the 27th of May to 00 UTC on the 19th of June 2016, including a spin-up time. The evaluation was conducted based on the observation data obtained at eight meteorological monitoring sites operated by the Korea Meteorological Administration (KMA). The statistical values, root mean square error (RMSE)/Index of Agreement (IOA), of modeling results were 1.97 °C/0.93 and 0.94 m s^{-1}/0.68 for temperature and wind speed, respectively.

2.7. Wind direction weighted concentrations (WWC)

The WWC was used to assess the impacts of local circulation in the source areas. The WWC was coupled with the surface wind direction data and calculated using Equation (1):

$$WWC = \frac{\sum_{i=1}^{N}(C_{\Delta\theta})WD_{\Delta\theta i}}{\sum_{i=1}^{N}WD_{\Delta\theta i}} \quad (1)$$

where $C_{\Delta\theta}$ is the concentration measured upon the arrival of the wind direction sector ($WD_{\Delta\theta}$); WWC (in μg/m^3 or ng/m^3 in $PM_{2.5}$) is the potential source direction strength; and N is the total number of $WD_{\Delta\theta}$. Eq. (1) was applied to $WD_{\Delta\theta}$ (i.e., $\Delta\theta = 30°$). After the redistribution, a new concentration field WWC was computed. To reduce the bias due to small numbers of $WD_{\Delta\theta}$ that cause in high WWC, a weight ($W_{\Delta\theta}$) (i.e., N times one tenth) was applied into the WWC to better reflect the values.

3. Results and discussions

Fig. 1 shows the time series of meteorological conditions (i.e., wind direction, wind speed, and temperature), ROS, OC, WSOC, ratio of WSOC to OC, EC, WSIs with ion charge balance, and five BCAs (i.e., 12BCA, 14BCA, 124BCA, 135BCA, and 1245BCA) in $PM_{2.5}$ from May 28 to June 20 in 2016. A total of 21 samples for ROS and

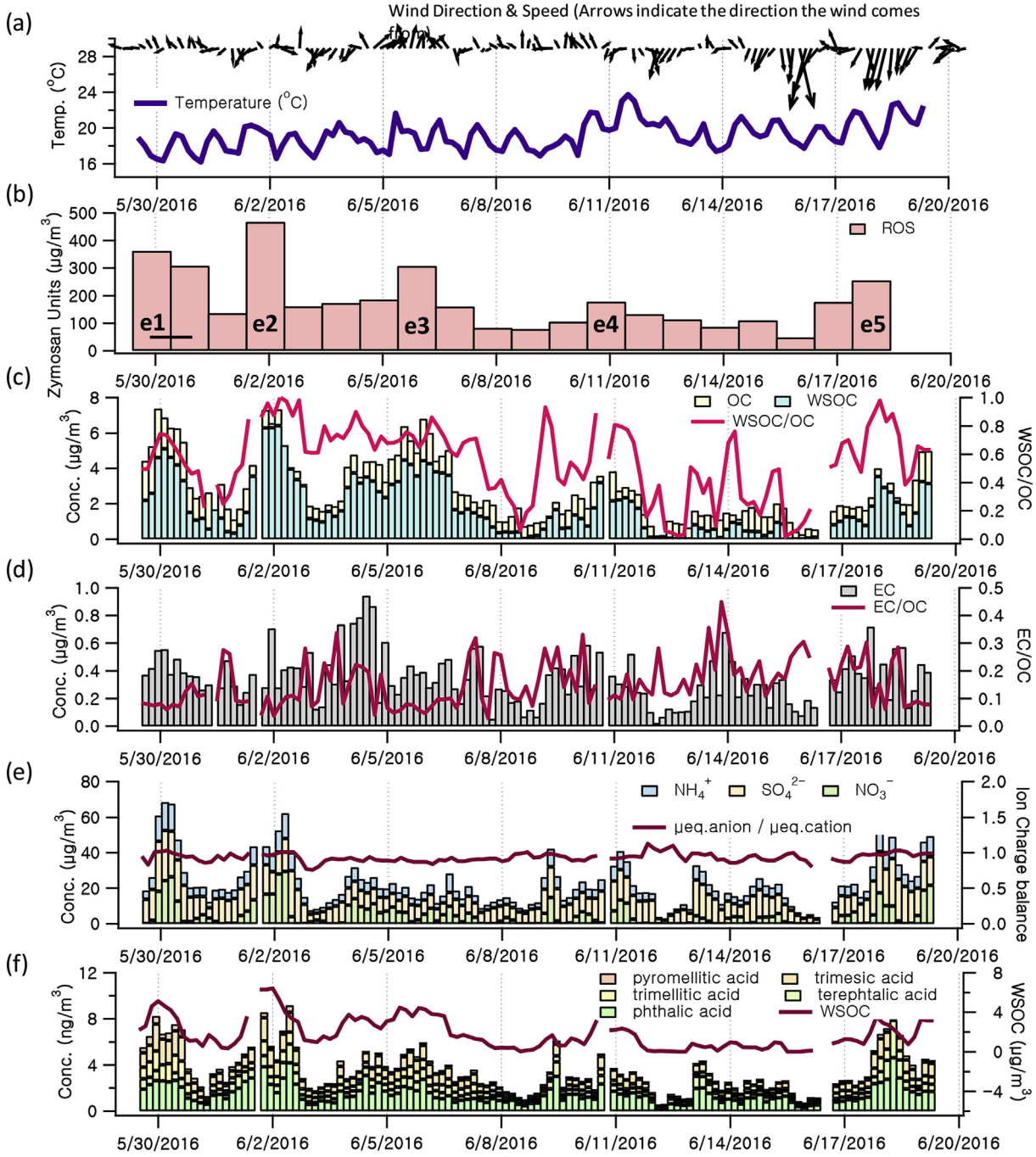

Fig. 1. (a) Time series of wind direction (arrows indicate the direction the wind comes from), wind speed, and temperature. (b) Time series of $PM_{2.5}$ reactive oxygen species (ROS). (c) Time series of organic carbon (OC), water-soluble organic carbon (WSOC), and the ratio of WSOC to OC. (d) Time series of elemental carbon (EC) and the ratio of EC to OC. (e) Time series of NO_3^-, SO_4^{2-}, NH_4^+, and ion charge balance. (f) Time series of underivatized phthalic acid (12BCA), terephtalic acid (14BCA), trimellitic acid (124BCA), trimesic acid (135BCA), pyromellitic acid (1245BCA), and WSOC in $PM_{2.5}$.

Table 1
Statistical concentration results of $PM_{2.5}$ ROS, OC, WSOC, EC, WSIs, BCAs, and trace elements for the sampling period.

	Unit	Sampling Days (N[a])	Mean	Standard Deviation	Maximum
ROS	μg/m^3 [b]	21 (21)	181	105	469
OC	μg/m^3	21 (120)	2.8	1.7	6.4
WSOC	μg/m^3	21 (121)	1.9	1.5	5.7
WIOC[c]	μg/m^3	21 (121)	1.0	0.4	2.2
EC	μg/m^3	21 (120)	0.4	0.1	0.6
EC/OC	–	21 (120)	0.1	0.1	0.3
NO_3^-	μg/m^3	21 (121)	4.7	4.6	18.9
SO_4^{2-}	μg/m^3	21 (121)	12.2	4.2	22.7
NH_4^+	μg/m^3	21 (121)	5.8	2.4	11.6
Mg^{2+}	μg/m^3	21 (121)	0.02	0.01	0.04
Ca^{2+}	μg/m^3	21 (121)	0.06	0.04	0.17
K^+	μg/m^3	21 (121)	0.13	0.21	0.98
12BCA	ng/m^3	21 (121)	1.48	0.57	2.68
14BCA	ng/m^3	21 (121)	0.50	0.18	0.82
124BCA	ng/m^3	21 (121)	0.53	0.32	1.40
135BCA	ng/m^3	21 (121)	0.78	0.42	1.85
1245BCA	ng/m^3	21 (121)	0.26	0.13	0.64
Al	ng/m^3	21 (21)	84	71	220
Si	ng/m^3	21 (21)	306	261	825
Fe	ng/m^3	21 (21)	149	104	317
Cu	ng/m^3	21 (21)	90	48	173
Mn	ng/m^3	21 (21)	9	9	27

[a] Number of Samples.
[b] Zymosan Unit.
[c] Differences between OC and WSOC.

trace elements were valid from 24-h integrated sampling. Numbers of 120 data for OC and EC, and 121 data for each WSI and BCA, were available with validations. Data was flagged and removed from the analysis if any of the following conditions were known (i.e., sampling activity and analytical instruments were out of extraction protocols, malfunctioning, and/or out of analytical quality assurance). Data completeness was over 96%, considering all sampling and analytical procedures. The macrophage ROS measurement results in Fig. 1 and Table 1 are expressed on a per air volume based activity metric in μg Zymosan units (ZU) per m^3. The overall average ROS concentration for the measurements was 181 ± 105 (average ± standard deviation) μg(ZU)/m^3. The measurements showed that the lowest ROS during the sampling period occurred on June 15. Fig. 1 shows that on the sampling date of June 1, the

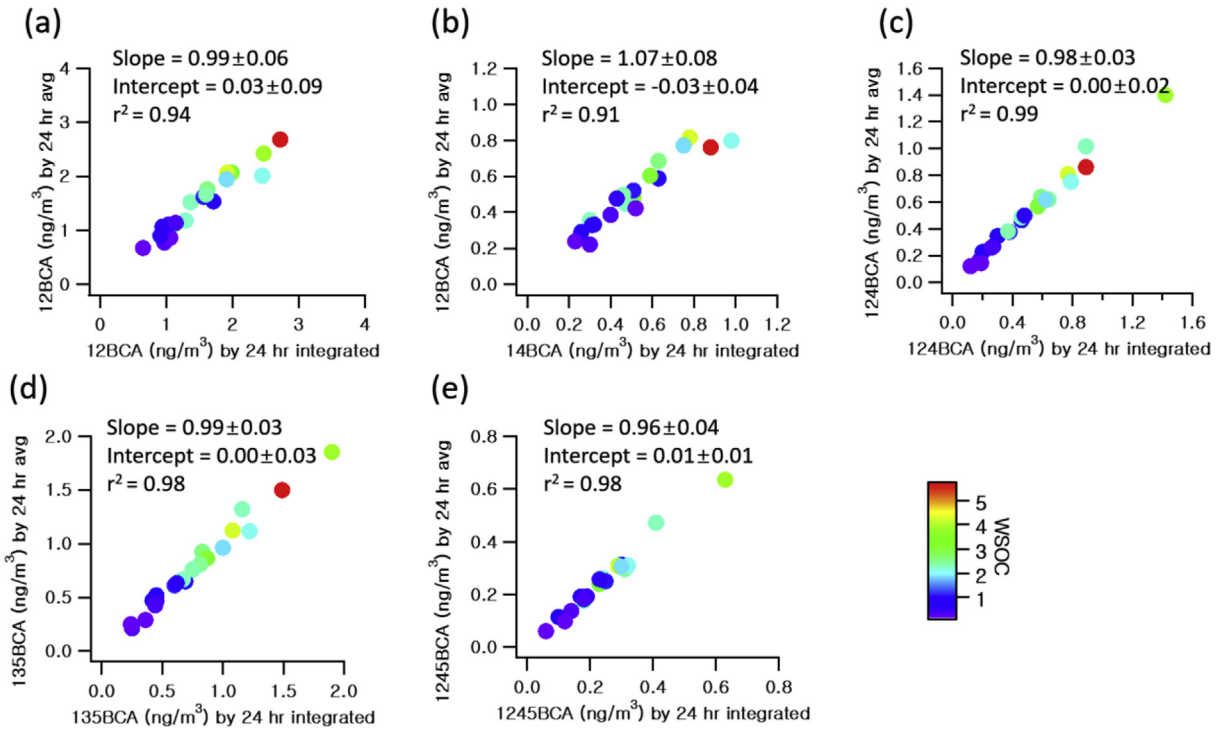

Fig. 2. Pairwise scatterplot between 24-h averaged concentrations of four-hour integrated samples using the custom-made $PM_{2.5}$ sequential sampler and 24-h integrated concentrations using the 24-h low volume sampler for underivatized (a) phthalic acid (12BCA), (b) terephtalic acid (14BCA), (c) trimellitic acid (124BCA), (d) trimesic acid (135BCA), and (e) pyromellitic acid (1245BCA) colored by water-soluble organic carbon (WSOC).

highest ROS was presented with an average of 469 μg(ZU)/m^3. The water insoluble concentrations of OC were estimated based on the differences between OC and WSOC from their carbon analyses. The average measured OC, WSOC, and EC concentrations in this study were 2.8 ± 1.7, 1.9 ± 1.7, and 0.4 ± 0.1 μgC/m^3, respectively. The averaged equivalent ratio of anions to cations was equal to 0.94. This indicates an incomplete neutralization of anion, due to the concurrent presence of $(NH_4)HSO_4$ and other hydrogen-containing ion compounds. The average SO_4^{2-}, NO_3^-, and NH_4^+ concentrations were 12.2 ± 4.2, 4.7 ± 4.6, and 5.8 ± 2.4 μg/m^3, respectively.

Analyses of time-resolved BCAs are important because they can provide informative applications for temporal issues related to source identifications and/or health effects. A large amount of coal combustion and biomass burning (e.g., both wildfire and households) in Northeast Asian countries enhances anthropogenic PM, which affects aerosol chemical composition in the remote atmosphere. Therefore, many primary organic compounds in Asian outflow can be photochemically oxidized to produce SOA during long-range transport (Bae et al., 2014). Only low molecular weight water-soluble organic compounds (i.e., diacids) have previously been identified (Deshmukh et al., 2016). However, time-resolved characteristics of BCAs have not been studied in the western North Pacific Rim. In this study, the average concentrations of 12BCA, 14BCA, 124BCA, 135BCA, and 1245BCA were 1.48 ± 0.57, 0.50 ± 0.18, 0.53 ± 0.32, 0.78 ± 0.42, and 0.26 ± 0.13 ng/m^3, respectively. The lowest and highest concentrations of BCAs were 1.3 and 6.1 ng/m^3 for the sampling period, which occurred on June 15 and June 1, respectively, the same days as ROS. Based on the good correlation ($r^2 = 0.76$) between the total BCAs and WSOC, the time-resolved chemical characteristics of these WSOC and BCAs imply their common origins.

Fig. 2 shows pairwise scatterplots between 24-h averaged BCAs from four-hour integrated samples using the $PM_{2.5}$ sequential sampler, and 24-h integrated BCAs using the 24-h low vol. sampler colored by WSOC. Excellent correlations were shown, and the slopes (between 0.96 ± 0.04 and 1.07 ± 0.08) are statistically indistinguishable from unity with high coefficients of correlation and determination (r^2 between 0.91 and 0.99). These results confirm that the underivatized analytical procedures (i.e., extractions, drying concentrations, and internal standard applications) can be assured, and the final concentrations can be safely validated. Organics denuders impregnated by activated black carbon have been utilized to reduce the positive artifacts related to the contribution of volatile organic compounds on quartz fiber filters.

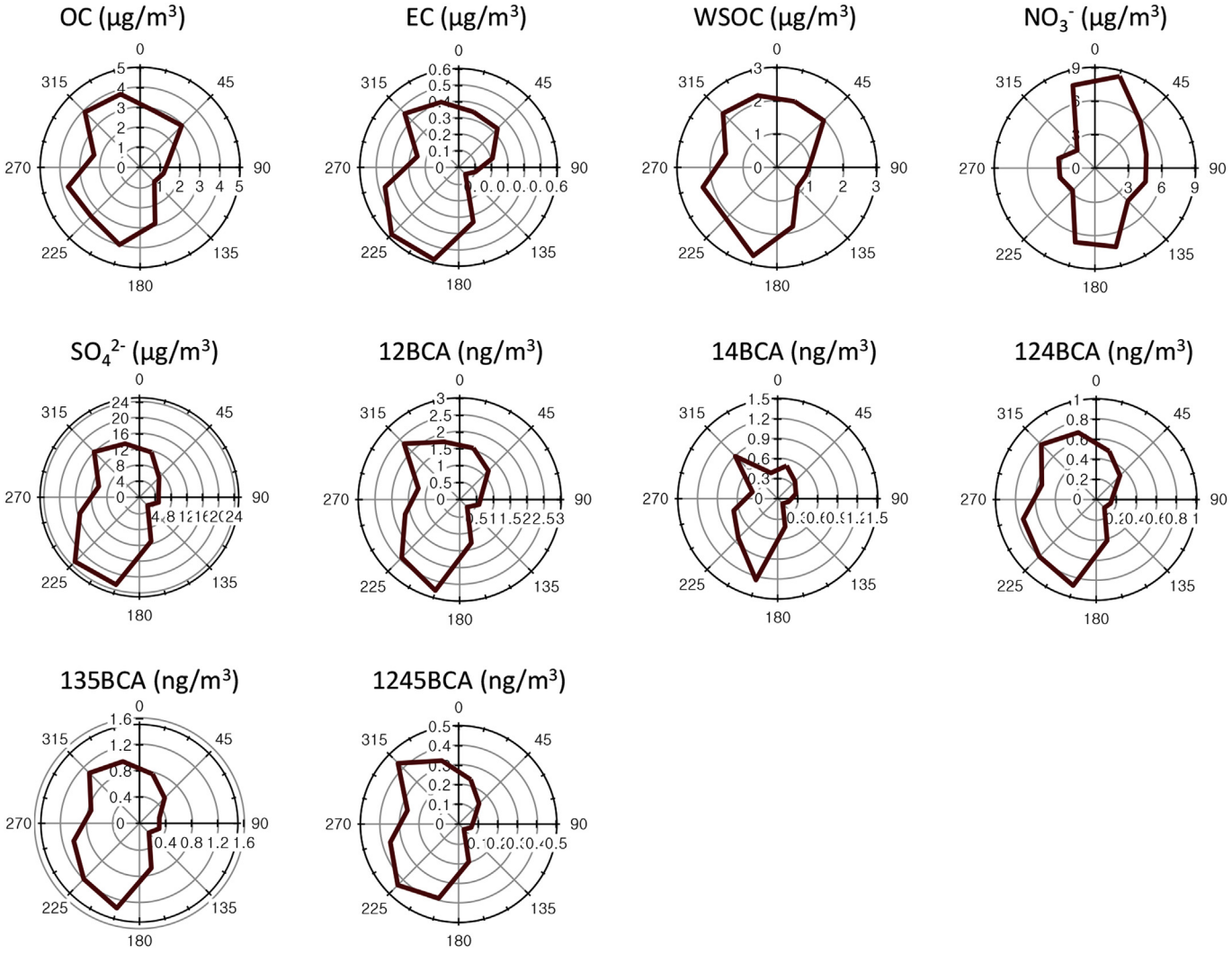

Fig. 3. Wind direction weighted concentration (WWC) polar plots of OC, EC, WSOC, NO_3^-, SO_4^{2-}, and BCAs (i.e., underivatized phthalic acid (12BCA), terephtalic acid (14BCA), trimellitic acid (124BCA), trimesic acid (135BCA), and pyromellitic acid (1245BCA)) in $PM_{2.5}$.

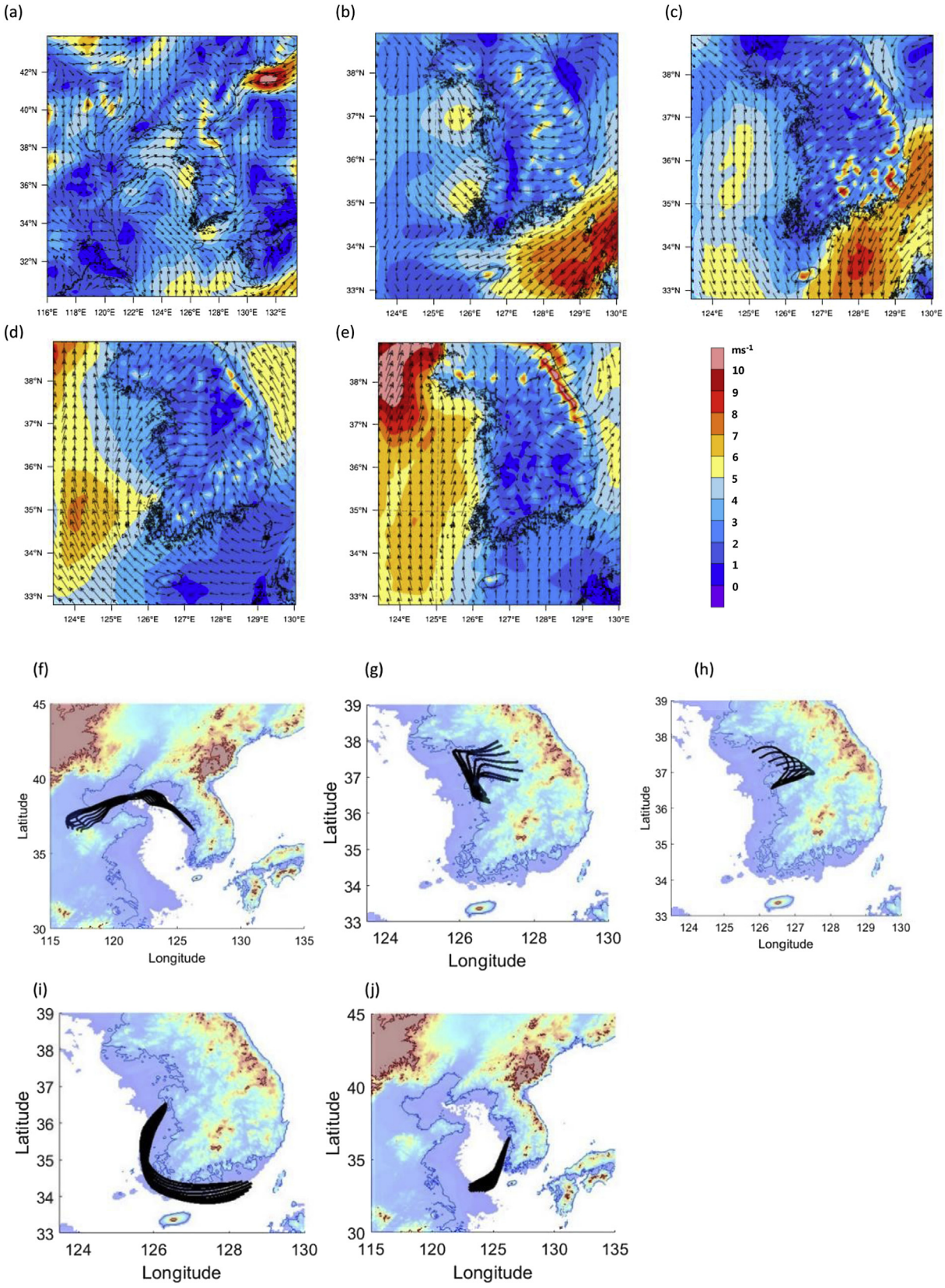

Fig. 4. Spatial distribution of meteorological conditions (i.e., wind direction and wind speed) using the Weather Research and Forecasting (WRF) model over Northwest Asia on (a) May 29, (b) June 1, (c) 5, (d) 10, and (e) 17, for e1, e2, e3, e4, and e5, respectively. Back trajectories of the air mass during the events (f) e1, (g) e2, (h) e3, (i) e4, and (j) e5. The color shows the geographical height. (For interpretation of the references to colour in this figure legend, the reader is referred to the web version of this article.)

However, only a few studies have investigated the performance of such denuders (Mader et al., 2003). There were good agreements between undenuded OC, EC, and WSOC using four-hour integrated $PM_{2.5}$ sequential sampler and denuded OC, EC, and WSOC using 24-h low volume sampler (Supplemental Fig. S2). For undenuded and denuded OC comparison, a linear regression shows a slope (forced to zero) of 1.35 ± 0.05 (slope ± standard error) and r^2 of 0.97. These results are compatible reported by Mader et al. (2003), showing that most of the OC positive artifact is associated with adsorption to the substrate. Fig. S2(b) compares undenuded and denuded EC concentrations. The slope for EC comparison is 1.02 ± 0.04 with r^2 of 0.97. These results illustrate that there are no significant artifacts for EC measurement using the denuder sampling. In addition, Fig. S2(c) shows that the denuded and undenuded WSOC correlate well with a slope of 1.06 ± 0.03 and r^2 of 0.98. In this case, organic acids with high molecular weights can be expected more (i.e., heterogeneous reactions consume organic acid more rapidly to higher molecular weight organic acids). This indicates that the role of organic acids in $PM_{2.5}$ at the receptor areas becomes of increasing importance.

Supplemental Fig. S3 shows diurnal variation of four-hour integrated measurement of OC, EC, EC/OC, WSOC, WSOC/OC, WSIs, and BCAs in $PM_{2.5}$. The OC, WSOC/OC, and SO_4^{2-} presented the feature of moderate diurnal pattern, which was maximal in the morning (08:00–12:00) and minimal at night, which can be explained by SOA formations influenced by changes in emissions. In contrast, NO_3^- was minimal in the middle of the day, due to thermodynamic properties (i.e., evaporation of ammonium nitrate) (Frank, 2006). Based on time-resolved samples using four-hour integrated sampling, the characteristic feature of BCA data sets present moderate diurnal patterns. The features of the 12BCA, 14BCA, and 135BCA distributions were the morning time (08:00–12:00) maximums, while 124BCA and 1245BCA distributions showed maximum concentrations during the middle of the day, due to photooxidation enhancement. The temporal pattern of the EC/OC ratio was different from that of the WSOC/OC ratio. A mono-distribution of the EC/OC ratio is in agreement with regional steady EC emission sources. The present study demonstrates the relative contributions of SOC to OC and/or WSOC at the sampling site, so this issue is being explored using molecular marker speciation (i.e., BCAs).

The WWC model based on measured wind direction was performed to identify the source origins of components of $PM_{2.5}$ based on measured wind direction. Fig. 3 shows the WWC results of OC, EC, WSOC, NO_3^-, SO_4^{2-}, and BCAs in $PM_{2.5}$. Meanwhile, conditional probability function (CPF), which stands for source directions at the sampling site (Lee and Hopke, 2006). The residence-time weighted concentrations (RTWC) approach was usually applied to the receptor site using back trajectories (Han et al., 2007). The WWC model was the combination of CPF and the RTWC model, which utilized the analyzed concentration distributions using the wind direction with weighted functions. The WWC in Fig. 3 shows that distinguishable directionalities for the emission sources of OC, EC, WSOC, NO_3^-, SO_4^{2-}, and BCAs. OC, WSOC, and BCAs presented two major source directions (i.e., the southwest and northwest). Only NO_3^- showed different distribution from north and south, with relatively large contributions in eastern directions. No statistically significant differences between day and night time WWCs for OC, WSOC, and BCAs were presented. This suggests that the boundary layer height are not of main impact, but the most influential factors are regional and/or long range transports into the site.

To investigate the relationship between ROS and analyzed compounds, Supplemental Table S3 shows the coefficient of determination (r^2) matrix between ROS, OC, EC, WSOC, WIOC, WSIs, and BCAs. This matrix indicates good coefficient of determinations between ROS and OC (r^2 of 0.82) and WSOC (r^2 of 0.81), with weak correlations with EC (r^2 of 0.25) and WIOC (r^2 of 0.21). In addition, good coefficients of determination between ROS and 124BCA and 135BCA were shown at 0.73 and 0.83, respectively.

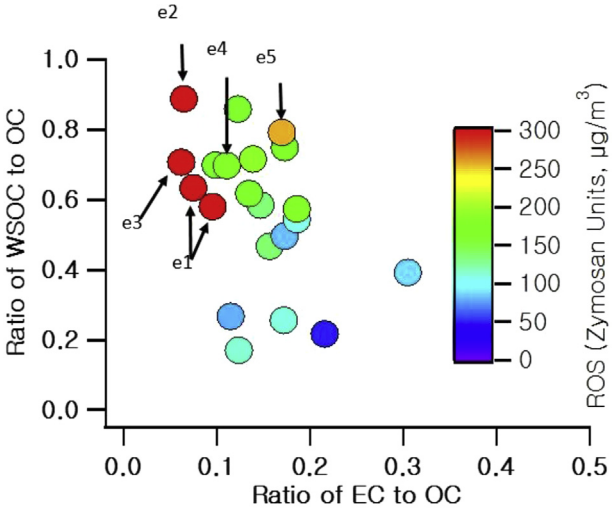

Fig. 6. Pairwise scatterplot between the ratio of WSOC to OC, and the ratio of EC to OC, colored by ROS.

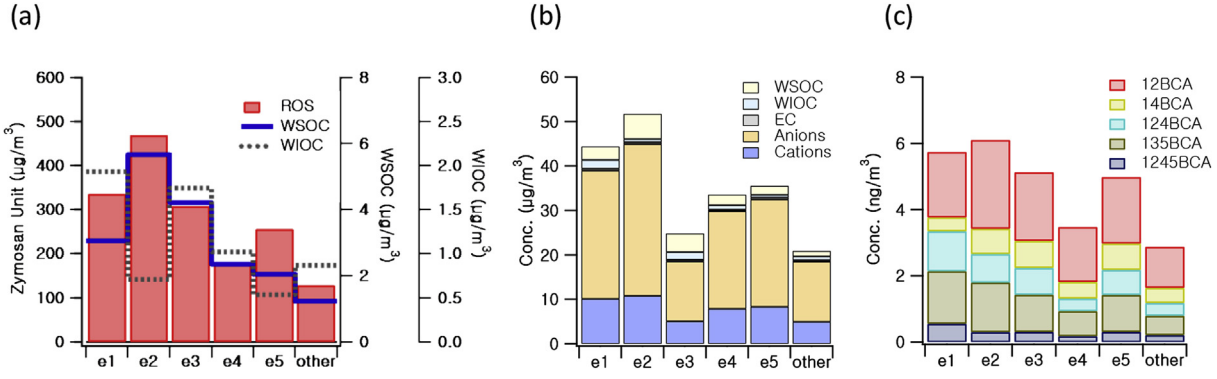

Fig. 5. Concentration of (a) ROS, WSOC, WIOC, (b) sum of WSOC, WIOC, EC, WSIs (i.e., anions and cations), and (c) sum of underivatized phthalic acid (12BCA), terephtalic acid (14BCA), trimellitic acid (124BCA), trimesic acid (135BCA), pyromellitic acid (1245BCA), and WSOC for event1 (e1), event2 (e2), event2 (e2), event3 (e3), event4 (e4), event5 (e5), and other (i.e., averaged concentrations excluding the selected event days) in $PM_{2.5}$.

For further analysis, five events were determined by plume events with high concentrations (i.e., ROS, OC, WSOC and BCAs concentrations, as shown in Fig. 1). The five selected event days were May 29–May 30, June 1, June 5, June 10, and June 17, labeled as e1, e2, e3, e4, and e5, respectively. For identification of the potential source areas, WRF and backward trajectory analyses were utilized during the selected events. Fig. 4(a)–(e) show the spatial distribution of meteorological conditions (i.e., wind direction and wind speed) using WRF over Northwest Asia. The contour color plots in Fig. 4(a)–(e) show the wind speeds (m/s). Fig. 4(f)–(j) show the back trajectories of the air mass during the events (e1–e5), as well. Selected times for the WRF model are those with the highest concentrations during each selected event. The wind distributions in grid cells indicate the horizontal and vertical advection/diffusion processes from potential source areas to the receptor site. Back trajectories of the air mass during the events (e1–e5) were shown as well in Fig. 4(f)–(j). Three-day and one-day air mass back trajectories were calculated for e1 and e2–e5, respectively, using the NOAA HYSPLIT model (Stein et al., 2015). Model results and observations clearly show that meteorological conditions play a key role in regulating PM concentrations in the lower troposphere through their regional and long-range transport variability. According to wind distributions and back trajectories, the increase of ROS concentrations clearly resulted in large part from the effects of meteorological conditions (the northwesterly (NW) and westerly (NW) winds) during the e1 period (Fig. 4(a)–(f)). The eastern areas of China (e.g., Cangzhou, Dongying, and Binzhou cities) throughout the northern region of the Yellow Sea can be high potential source

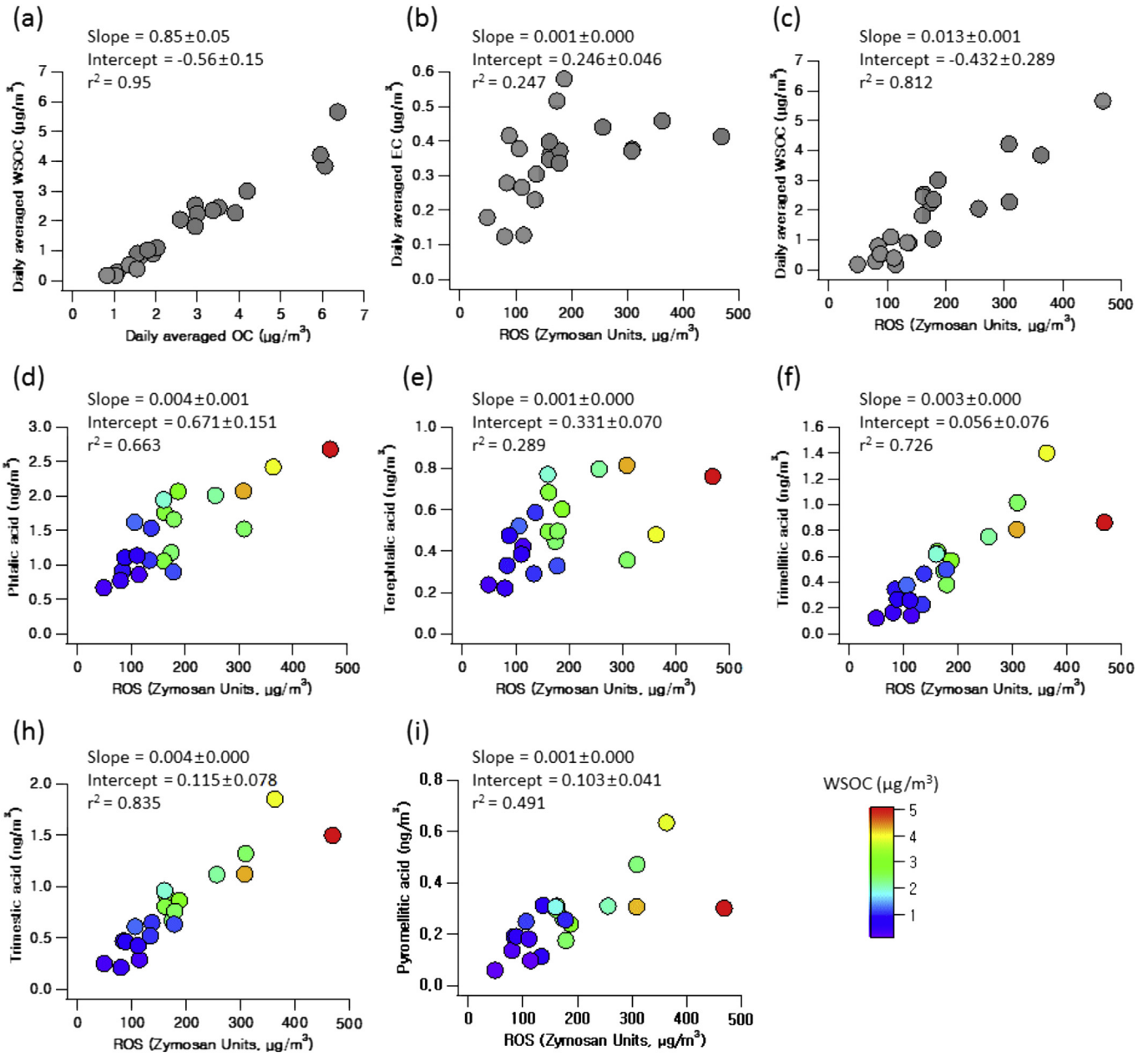

Fig. 7. Pairwise scatterplot between (a) daily averaged WSOC and OC, (b) EC and ROS, and (c) WSOC and ROS. Pairwise scatterplot between underivatized (d) phthalic acid (12BCA) and ROS, (e) terephtalic acid (14BCA) and ROS, (f) trimellitic acid (124BCA) and ROS, (h) trimesic acid (135BCA) and ROS, and (i) pyromellitic acid (1245BCA) and ROS, colored by WSOC in $PM_{2.5}$.

areas to the receptor site during the e1 period. Wind distributions and back trajectories during the e2 and e3 periods presented the regional whirlwind patterns in the northern region of the sampling site. The ROS concentrations were related to the regional sources in the middle of the Korean Peninsula with the interaction of secondary productions. Wind distributions and back trajectories during e4 and e5 showed somewhat different patterns from those during e1 and e3. The southern and south-western regions of Korea, including the southern region of the Yellow Sea, have higher probabilities of potential ROS source areas. Therefore, the concentration differences were likely related in large part to the meteorological conditions (Fig. 4). For example, the main wind direction for each event did not change during the event.

Fig. 5 shows the concentrations of ROS, WSOC, WIOC, sum of underivatized BCAs, and other (i.e., averaged concentrations excluding the selected event days) in $PM_{2.5}$. The ROS concentrations for e1–e5 were 336, 469, 308, 179, and 256 μg(ZU)/m^3, respectively, which were about 1.4–3.7 times higher than other (128 μg(ZU)/m^3). The patterns of WSOC concentrations were very similar to those of ROS, whereas those of WIOC were not, as shown in Fig. 5(a). In addition, the sums of underivatized BCA concentrations were 5.7, 6.1, 5.1, 3.5, and 5.0 ng/m^3 for e1–e5, respectively. These BCA patterns were clearly following the ROS. Fig. 7(c) shows that the daily averaged WSOC and ROS correlate well with 0.013 ± 0.001 (slope ± standard error) r^2 of 0.81, while Fig. 7(b) shows bad correlation between the daily averaged EC and ROS. These results demonstrate that ROS and EC did not show significant associations. This relationship implies that the toxicity intensities between ROS and WSOC can be more important than those of measured insoluble compounds. This can allow informative application to be gained on health associated with water-soluble chemical compounds of aerosols in Asian outflow. Fig. 6 shows the pairwise scatterplot between the ratio of WSOC to OC and the ratio of EC to OC colored by ROS to support their relations. Fig. 6 definitely shows two rims, which are high WSOC/OC with low EC/OC, and low WSOC/OC with high EC/OC. All e1–e5, which have high ROS concentrations, were laid in the rim of high WSOC/OC with low EC/OC. To investigate the detailed relationships between ROS and analyzed BCA compounds, Fig. 7 shows pairwise scatterplots between each BCA compound and ROS colored by WSOC. Good correlations between the daily averaged 12BCA, 124BCA, and 135BCA and ROS were shown as 0.67 ± 0.15 (r^2 of 0.66), 0.003 ± <0.000 (r^2 of 0.73), and 0.004 ± <0.000 (r^2 of 0.84), respectively. 14BCA and 1245BCA showed positive, weak or moderate correlations with ROS, with r^2 of 0.29 and 0.49, respectively. While we do not clearly understand the relationship differences between ROS and each BCA compound, it is clear that all ROS relationships with BCA are consistent with the patterns of WSOC concentrations. We believe that additional organic acids can be expected based on heterogeneous oxygen attacking reactions by photochemical process from their variety originations. The presence of time-resolved organic acids including discussed BCAs can be researched to find the relationship with ROS for further study.

Typical secondary electron images (SEIs) of $PM_{2.5}$ particles collected during the event periods, except the e5 period when no sampling activity for SEM/EDX analysis was performed, are shown in Fig. 8, where the chemical species making up each particle are also indicated. The chemical species of individual particles were determined by the analysis of their X-ray spectra. As shown in Fig. 8, various types of particles were observed, including mixture particles of organics and ammonium sulfates, organic particles, reacted (aged) sea salts, aluminosilicates, $CaCO_3$, and $CaSO_4$, which are denoted on the SEIs as “COS”, “org”, “rss”, “AlSi”, “$CaCO_3$”, and “$CaSO_4$”, respectively. Although the four samples collected during the event periods have somewhat different chemical compositions (i.e., “AlSi” and “rss” particles are observed more in the samples

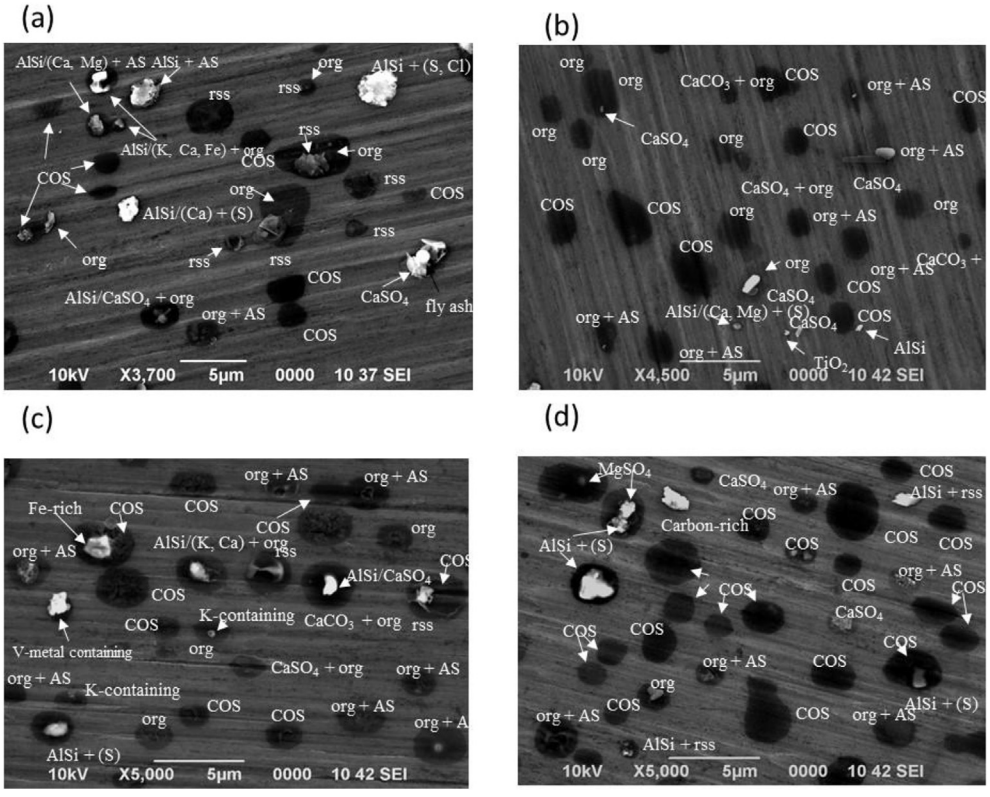

Fig. 8. Secondary electron imagery (SEI) in $PM_{2.5}$ during (a) e1, (b) e2, (c) e3, and (d) e4 periods.

collected during the e1 and e3 periods than those during the e2 and e4 periods), "COS" and "org" particle types are prominent for all the event samples. As the "COS" and "org" particles look dark in contrast and somewhat round in shape on their SEI, their morphological "footprints" on SEI indicate that they were collected as aqueous droplets at the time of sampling (Geng et al., 2009, 2014). The "COS" particles with major C, O, and S components are the mixture of water-soluble organic carbon with ammonium sulfates and the "org" particles with major C and O components are mainly composed of water-soluble organic carbon (Geng et al., 2009, 2014). Based on the observation of droplet particles containing WSOC by the SEM/EDX single-particle analysis, it is clear that water-soluble compounds are abundant in $PM_{2.5}$ collected during the event periods.

4. Conclusions

This study characterized the time-resolved main chemical compositions of aerosol particles collected between May 28 and June 20 of 2016 at a west coastal site in the Republic of Korea, and investigated the relationship between water-soluble organic compounds and ROS using a fluorogenic cell-based method in rat alveolar macrophages during the KORea-US Air Quality (KORUS-AQ) campaign. Four-hour time-resolved integrated samples, including OC and EC, WSOC, WSIs, and five BCA compounds, were collected using a custom-made sequence sampler controlled by an MFC and were analyzed by SUNET carbon analyzer, TOC, IC, and LC-MSMS, respectively. The WRF model and air mass back trajectory analysis indicated the influence of both regional and long-range transport during the selected events. Good coefficients of determination between ROS and OC (r^2 of 0.82), WSOC (r^2 of 0.81), 124BCA (r^2 of 0.73), and 135BCA (r^2 of 0.83) demonstrate that the toxicity intensities between ROS and water-soluble compounds can be more important than those of the measured insoluble compounds. This can allow informative application to be gained on health associated with water-soluble chemical compounds of aerosols in Asian outflow. In addition, their morphologies on SEI, which were in the form of water droplets, implies that the types of particles were likely the droplets containing WSOC and confirmed the presence of water-soluble compounds in $PM_{2.5}$.

Acknowledgments

We acknowledge the support of the National Research Foundation of Korea (NRF) (NRF-2015R1A2A1A10053971).

Appendix A. Supplementary data

Supplementary data related to this article can be found at http://dx.doi.org/10.1016/j.envpol.2017.07.100.

References

Agudelo-Castañeda, D.M., Teixeira, E.C., Schneider, I.L., Lara, S.R., Silva, L.F.O., 2017. Exposure to polycyclic aromatic hydrocarbons in atmospheric PM1.0 of urban environments: carcinogenic and mutagenic respiratory health risk by age groups. Environ. Pollut. 224, 158–170.

Bae, M.-S., Lee, J.-Y., Kim, Y.-P., Oak, M.-H., Shin, J.-S., Lee, K.-Y., Lee, H.-H., Lee, S.-Y., Kim, Y.-J., 2012. Analytical methods of levoglucosan, a tracer for cellulose in biomass burning, by four different techniques. Asian J. Atmos. Environ. 6, 53–66.

Bae, M.-S., Schauer, J.J., DeMinter, J.T., Turner, J.R., 2004a. Hourly and daily patterns of particle-phase organic and elemental carbon concentrations in the urban atmosphere. Air & Waste Manag. Assoc. 54, 823–833.

Bae, M.-S., Schauer, J.J., DeMinter, J.T., Turner, J.R., Smith, D., Cary, R.A., 2004b. Validation of a semi-continuous instrument for elemental carbon and organic carbon using a thermal-optical method. Atmos. Environ. 38, 2885–2893.

Bae, M.-S., Schauer, J.J., Turner, J.R., 2006. Estimation of the monthly average ratios of organic mass to organic carbon for fine particulate matter at an urban site. Aerosol Sci. Technol. 40, 1123–1139.

Bae, M.S., Shin, J.S., Lee, K.Y., Lee, K.H., Kim, Y.J., 2014. Long-range transport of biomass burning emissions based on organic molecular markers and carbonaceous thermal distribution. Sci. Total Environ. 466–467, 56–66.

Belis, C.A., Cancelinha, J., Duane, M., Forcina, V., Pedroni, V., Passarella, R., Tanet, G., Douglas, K., Piazzalunga, A., Bolzacchini, E., Sangiorgi, G., Perrone, M.G., Ferrero, L., Fermo, P., Larsen, B.R., 2011. Sources for PM air pollution in the Po Plain, Italy: I. Critical comparison of methods for estimating biomass burning contributions to benzo(a)pyrene. Atmos. Environ. 45, 7266–7275.

Campbell, A., Oldham, M., Becaria, A., Bondy, S.C., Meacher, D., Sioutas, C., Misra, C., Mendez, L.B., Kleinman, M., 2005. Particulate matter in polluted air May increase biomarkers of inflammation in mouse brain. NeuroToxicology 26, 133–140.

Deshmukh, D.K., Kawamura, K., Lazaar, M., Kunwar, B., Boreddy, S.K.R., 2016. Dicarboxylic acids, oxoacids, benzoic acid, α-dicarbonyls, WSOC, OC, and ions in spring aerosols from Okinawa Island in the western North Pacific Rim: size distributions and formation processes. Atmos. Chem. Phys. 16, 5263–5282.

Frank, N.H., 2006. Retained nitrate, hydrated sulfates, and carbonaceous mass in federal reference method fine particulate matter for six eastern U.S. cities. Air & Waste Manag. Assoc. 56, 500–511.

Geng, H., Hwang, H., Liu, X., Dong, S., Ro, C.U., 2014. Investigation of aged aerosols in size-resolved Asian dust storm particles transported from Beijing, China, to Incheon, Korea, using low-Z particle EPMA. Atmos. Chem. Phys. 14, 3307–3323.

Geng, H., Jung, H.-J., Park, Y., Hwang, H., Kim, H., Kim, Y.J., Sunwoo, Y., Ro, C.-U., 2009. Morphological and chemical composition characteristics of summertime atmospheric particles collected at Tokchok Island, Korea. Atmos. Environ. 43, 3364–3373.

Hamad, S.H., Shafer, M.M., Kadhim, A.K.H., Al-Omran, S.M., Schauer, J.J., 2015. Seasonal trends in the composition and ROS activity of fine particulate matter in Baghdad, Iraq. Atmos. Environ. 100, 102–110.

Han, Y.-J., Holsen, T.M., Hopke, P.K., 2007. Estimation of source locations of total gaseous mercury measured in New York State using trajectory-based models. Atmos. Environ. 41, 6033–6047.

Hasheminassab, S., Daher, N., Schauer, J.J., Sioutas, C., 2013. Source apportionment and organic compound characterization of ambient ultrafine particulate matter (PM) in the Los Angeles Basin. Atmos. Environ. 79, 529–539.

Ho, K.F., Ho, S.S.H., Lee, S.C., Kawamura, K., Zou, S.C., Cao, J.J., Xu, H.M., 2011. Summer and winter variations of dicarboxylic acids, fatty acids and benzoic acid in PM2.5 in Pearl Delta River Region, China. Atmos. Chem. Phys. 11, 2197–2208.

Jeon, W., Choi, Y., Lee, H.W., Lee, S.-H., Yoo, J.-W., Park, J., Lee, H.-J., 2015. A quantitative analysis of grid nudging effect on each process of PM2.5 production in the Korean Peninsula. Atmos. Environ. 122, 763–774.

Jordan, T.B., Seen, A.J., Jacobsen, G.E., 2006. Levoglucosan as an atmospheric tracer for woodsmoke. Atmos. Environ. 40, 5316–5321.

Jung, J., Kim, Y.J., Aggarwal, S.G., Kawamura, K., 2011. Hygroscopic property of water-soluble organic-enriched aerosols in Ulaanbaatar, Mongolia during the cold winter of 2007. Atmos. Environ. 45, 2722–2729.

Kautzman, K.E., Surratt, J.D., Chan, M.N., Chan, A.W.H., Hersey, S.P., Chhabra, P.S., Dalleska, N.F., Wennberg, P.O., Flagan, R.C., Seinfeld, J.H., 2010. Chemical composition of gas- and aerosol-phase products from the photooxidation of naphthalene. J. Phys. Chem. A 114, 913–934.

Kawamura, K., Kaplan, I.R., 1987. Motor exhaust emissions as a primary source for dicarboxylic acids in Los Angeles ambient air. Environ. Sci. Technol. 21, 105–110.

Kawamura, K., Kasukabe, H., Barrie, L.A., 1996. Source and reaction pathways of dicarboxylic acids, ketoacids and dicarbonyls in arctic aerosols: one year of observations. Atmos. Environ. 30, 1709–1722.

Kleindienst, T.E., Jaoui, M., Lewandowski, M., Offenberg, J.H., Docherty, K.S., 2012. The formation of SOA and chemical tracer compounds from the photooxidation of naphthalene and its methyl analogs in the presence and absence of nitrogen oxides. Atmos. Chem. Phys. 12, 8711–8726.

Landreman, A.P., Shafer, M.M., Hemming, J.C., Hannigan, M.P., Schauer, J.J., 2008. A macrophage-based method for the assessment of the reactive oxygen species (ROS) activity of atmospheric particulate matter (PM) and application to routine (Daily-24 h) aerosol monitoring studies. Aerosol Sci. Technol. 42, 946–957.

Lee, J.H., Hopke, P.K., 2006. Apportioning sources of PM2.5 in St. Louis, MO using speciation trends network data. Atmos. Environ. 40 (Suppl. 2), 360–377.

Mader, B.T., Schauer, J.J., Seinfeld, J.H., Flagan, R.C., Yu, J.Z., Yang, H., Lim, H.-J., Turpin, B.J., Deminter, J.T., Heidemann, G., Bae, M.S., Quinn, P., Bates, T., Eatough, D.J., Huebert, B.J., Bertram, T., Howell, S., 2003. Sampling methods used for the collection of particle-phase organic and elemental carbon during ACE-Asia. Atmos. Environ. 37, 1435–1449.

Morgan, T.E., Davis, D.A., Iwata, N., Tanner, J.A., Snyder, D., Ning, Z., Kam, W., Hsu, Y.-T., Winkler, J.W., Chen, J.-C., Petasis, N.A., Baudry, M., Sioutas, C., Finch, C.E., 2011. Glutamatergic neurons in rodent models respond to nanoscale particulate urban air pollutants in vivo and in vitro. Environ. Health Perspect. 119, 1003–1009.

Pant, P., Yin, J., Harrison, R.M., 2014. Sensitivity of a Chemical Mass Balance model to different molecular marker traffic source profiles. Atmos. Environ. 82, 238–249.

Pathak, R.K., Wang, T., Ho, K.F., Lee, S.C., 2011. Characteristics of summertime PM2.5 organic and elemental carbon in four major Chinese cities: implications of high acidity for water-soluble organic carbon (WSOC). Atmos. Environ. 45, 318–325.

Ro, C.-U., Kim, H., Van Grieken, R., 2004. An expert system for chemical speciation of individual particles using low-z particle electron probe x-ray microanalysis data. Anal. Chem. 76, 1322–1327.

Ro, C.-U., Osán, J., Szalóki, I., de Hoog, J., Worobiec, A., Grieken, R.V., 2003. A monte carlo program for quantitative electron-induced x-ray analysis of individual particles. Anal. Chem. 75, 851–859.

Rogge, W.F., Hildemann, L.M., Mazurek, M.A., Cass, G.R., Simoneit, B.R.T., 1997. Sources of fine organic aerosol. 8. Boilers burning No. 2 distillate fuel oil. Environ. Sci. Technol. 31, 2731–2737.

Saxena, P., Hildemann, L.M., 1996. Water-soluble organics in atmospheric particles: a critical review of the literature and application of thermodynamics to identify candidate compounds. J. Atmos. Chem. 24, 57–109.

Simoneit, B.R.T., Kobayashi, M., Mochida, M., Kawamura, K., Huebert, B.J., 2004. Aerosol particles collected on aircraft flights over the northwestern Pacific region during the ACE-Asia campaign: composition and major sources of the organic compounds. J. Geophys. Res. Atmos. 109 http://dx.doi.org/10.1029/2004JD004565.

Snyder, D.C., Rutter, A.P., Collins, R., Worley, C., Schauer, J.J., 2009. Insights into the origin of water soluble organic carbon in atmospheric fine particulate matter. Aerosol Sci. Technol. 43, 1099–1107.

Stein, A.F., Draxler, R.R., Rolph, G.D., Stunder, B.J.B., Cohen, M.D., Ngan, F., 2015. NOAA's HYSPLIT atmospheric transport and dispersion modeling system. Bull. Am. Meteorol. Soc. 96, 2059–2077.

Stone, E.A., Zhou, J., Snyder, D.C., Rutter, A.P., Mieritz, M., Schauer, J.J., 2009. A comparison of summertime secondary organic aerosol source contributions at contrasting urban locations. Environ. Sci. Technol. 43, 3448–3454.

Sullivan, A.P., Weber, R.J., Clements, A.L., Turner, J.R., Bae, M.S., Schauer, J.J., 2004. A method for on-line measurement of water-soluble organic carbon in ambient aerosol particles: results from an urban site. Geophys. Res. Lett. 31 http://dx.doi.org/10.1029/2004GL019681.

Tuet, W.Y., Fok, S., Verma, V., Tagle Rodriguez, M.S., Grosberg, A., Champion, J.A., Ng, N.L., 2016. Dose-dependent intracellular reactive oxygen and nitrogen species (ROS/RNS) production from particulate matter exposure: comparison to oxidative potential and chemical composition. Atmos. Environ. 144, 335–344.

Verma, V., Rico-Martinez, R., Kotra, N., King, L., Liu, J., Snell, T.W., Weber, R.J., 2012. Contribution of water-soluble and insoluble components and their hydrophobic/hydrophilic subfractions to the reactive oxygen species-generating potential of fine ambient aerosols. Environ. Sci. Technol. 46, 11384–11392.

Wang, D., Pakbin, P., Shafer, M.M., Antkiewicz, D., Schauer, J.J., Sioutas, C., 2013. Macrophage reactive oxygen species activity of water-soluble and water-insoluble fractions of ambient coarse, PM2.5 and ultrafine particulate matter (PM) in Los Angeles. Atmos. Environ. 77, 301–310.

Xia, T., Korge, P., Weiss, J.N., Li, N., Venkatesen, M.I., Sioutas, C., Nel, A., 2004. Quinones and aromatic chemical compounds in particulate matter induce mitochondrial dysfunction: implications for ultrafine particle toxicity. Environ. Health Perspect. 112, 1347–1358.

Yan, C., Zheng, M., Sullivan, A.P., Bosch, C., Desyaterik, Y., Andersson, A., Li, X., Guo, X., Zhou, T., Gustafsson, Ö., Collett Jr., J.L., 2015. Chemical characteristics and light-absorbing property of water-soluble organic carbon in Beijing: biomass burning contributions. Atmos. Environ. 121, 4–12.